M&C 2017 - International Conference on Mathematics & Computational Methods Applied to Nuclear Science & Engineering, Jeju, Korea, April 16-20, 2017, on USB (2017)

Resonance Self-shielding Methods for Pin-resolved Direct Transport in LWR calculations

Yuxuan Liu and William Martin

Department of Nuclear Science and Engineering, University of Michigan: 2355 Bonisteel Blvd. Ann Arbor, MI, 48105
yuxuanl@umich.edu; wrm@umich.edu

Abstract - *An essential component of the deterministic reactor core analysis is the resonance self-shielding calculation, which is used to produce problem-specific multigroup cross sections. Equivalence theory and the subgroup method have been widely used to perform this task in the conventional two-step core analysis. However, recent progress with high-fidelity whole core direct transport methodology sets up new requirements for the associated self-shielding method, namely, being able to resolve within-pin effects such as multi-region depletion and non-uniform fuel temperature distribution. In the framework of whole core direct transport, the usability of existing self-shielding methods needs to be reexamined, and advanced self-shielding methods should be proposed to allow these new requirements to be met. This paper reviews the important physics of resonance self-shielding that should be properly modeled in direct transport calculation, including spatial self-shielding effects, resonance interference, non-uniform temperature effects and clad self-shielding. We discuss the qualification of four self-shielding methods, i.e., equivalence theory, the physical subgroup method, ESSM and ESSM-X, in handling the basic and advanced requirements. The computational resources of these methods are also compared.*

I. INTRODUCTION

In deterministic reactor core analysis, the multigroup (MG) approximation is usually used to treat the complicated energy behavior of resonance cross sections. The conventional reactor core analysis utilizes a two-step methodology. The two-step approach has been necessitated over the years because of the computational burden of dealing with the extreme energy dependence of cross sections and the geometric complexity of a full core reactor. Given a suitable fine-group library of cross sections from a library generation code such as NJOY [1] or AMPX [2], the first step is the lattice calculation that starts with the resonance self-shielding calculation to produce problem-specific MG cross sections. Those cross sections are then condensed into few groups and homogenized over the lattice (e.g., full assembly or 1/4 assembly) for the full core diffusion calculation in the second step. In contract to the two-step method, modern direct whole-core transport methods perform a transport calculation using the realistic geometry, material composition, and temperature profile of the reactor configuration. However, evaluating the problem-dependent MG effective cross sections for the explicit configuration (i.e., the resonance calculation) is still an essential task to assure the accuracy of the direct transport method.

To avoid the expensive calculation of the continuous-energy (CE) slowing-down equation for a fuel lattice, a number of physical and mathematical approximations have been developed for the resonance calculation [3]. Although some of the resonance methods developed for the lattice calculation can be incorporated into the direct transport method, the latter requires additional considerations for the pin-resolved capabilities of a 'high-fidelity' calculation, such as the within-pin depletion and thermal feedback [4]. This paper discusses the qualification of four typical methods in handling the basic and advanced requirements in the resonance calculation. Three resonance methods widely used in the current lattice and whole-core transport codes are reviewed, including equivalence theory [5], the physical subgroup method [6] (referred to as subgroup method for simplicity in the rest of the paper) and the embedded self-shielding method (ESSM) [7,8]. A new method ESSM-X [9] recently implemented into the CASL direct transport neutronics solver MPACT [10] is also discussed.

II. PHYSICS OF SELF-SHIELDING

The following physics phenomena that are important for the resonance calculation are reviewed: spatial self-shielding effects, resonance interference, non-uniform temperature profiles and clad self-shielding. ESSM-X, which addresses these phenomena, is briefly reviewed at the end of this section.

1. Spatial Self-shielding Effects

Spatial self-shielding is conventionally modeled by equivalence theory, which correlates the heterogeneous problem with a homogeneous resonance integral (RI) table by adding the equivalence cross section Σ_{eq} into the background cross section,

$$\sigma_{b,res} = \left(\sum_{iso} \lambda_{iso} \Sigma_{p,iso} + \Sigma_{eq} \right) \Big/ N_{res} \,. \qquad (1)$$

There are several approximations that could lead to formulas similar to Eq. (1), but here the single-term rational approximation [11] and the intermediate resonance approximation [12] are used. The equivalence cross section differs in each pin location due to neighboring shielding effects, thus variations of effective cross sections can be obtained by interpolating the background cross section through the RI table. In addition to the inter-pin effect, modeling the within-pin effect is also needed in the direct transport calculation.

Fig. 1 shows a typical Westinghouse 17×17 PWR assembly with inter-assembly water gap. In Fig. 2, the U-238 absorption rates of the three pin locations (each with ten rings of fuel) are compared with MCNP calculations [13]. The inter-pin effect is easily seen by examining Pins 1-3. Because of the larger equivalence cross section introduced by proximity to the water hole/gap, Pin 3 has the largest equivalence cross section followed by Pin 1. As a result, the effective absorption rates of Pin 1 for all fuel rings are slightly larger than those of Pin 2, and Pin 3 has the largest absorption rates of the three pins. The within-pin effect can be also be seen In Fig. 2, as each pin sees a large gradient of U-238 absorption rates from fuel surface to center, leading to the rim effect as the fuel depletes.

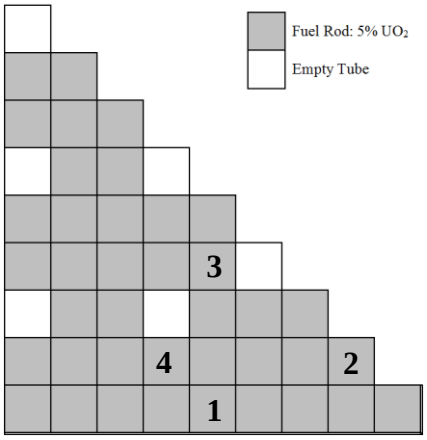

Fig. 1 PWR assembly with inter-assembly water gap

Although there is a theoretical limitation in applying both the multi-term rational approximation and the intermediate resonance approximation [5,14], the accuracy of modeling inter-pin effects by equivalence theory is generally acceptable. However, an asymptotic study shows that the rational approximation cannot work for a multiple-ring fuel region [15]. Therefore, conventional equivalence theory and ESSM, which depends on equivalence theory, cannot model the within-pin reaction rate distribution correctly. The multiple fuel region escape probability should be calculated by extending the rational type approximation [15,16]. If the conventional rational form is still desired, an energy dependent equivalence cross section is needed. On the other hand, the subgroup method effectively computes an energy-dependent equivalence cross section via subgroup levels, so a better representation of the within-pin effect is achieved by the subgroup method. Numerical verification of these observations will be discussed in Section III.

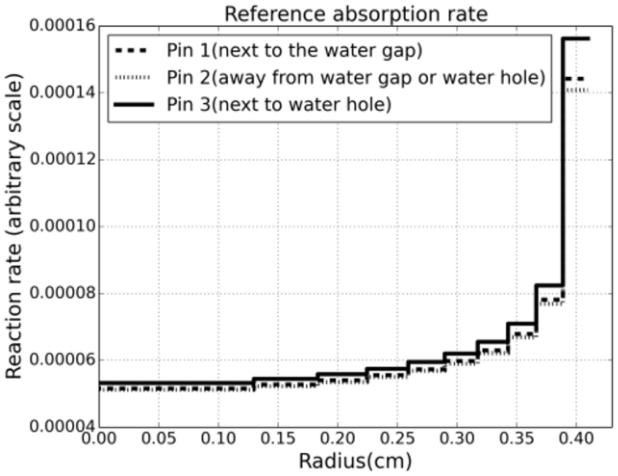

Fig. 2 Spatially dependent absorption rates of U-238 for Pins 1, 2 and 3

We've discussed the within-pin effect along the radial direction. In some circumstances, reaction rates could vary significantly in the azimuthal direction. For instance, Pin 4 in Fig. 1 has a strong azimuthal heterogeneity. We ran MCNP for Pin 4 with an azimuthally refined mesh shown in Fig. 3. The U-238 effective absorption cross sections and rates of subregions 1 and 3 computed by MCNP using a 56-group energy structure [17] are shown in Fig. 4. Differences in the range 4%~15% are observed for the effective cross sections in major resonance groups for Subregions 1 and 3, while 10%~35% differences are observed for the reaction rates. Interestingly, for large resonances such as the U-238 6.67eV, the difference in effective cross sections between Subregions 1 and 3 is small, but the difference in reaction rate is large, indicating the latter is primarily due to the difference in neutron flux. As reaction rate is our major concern, a precise azimuthal model for cross section is appreciated, but is not a mandatory requirement. As will be shown in Section III, the azimuthal effect can be accurately modeled by the subgroup method, while the results of ESSM/ESSM-X are acceptable even they are less accurate in handling the azimuthally varied cross sections.

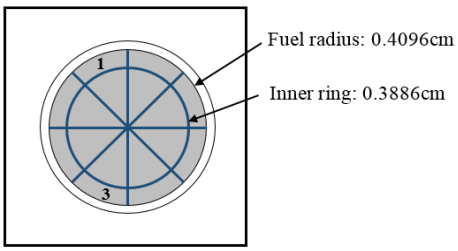

Fig. 3 Within-pin mesh for investigating azimuthal effect (region 1 is closer to the water hole)

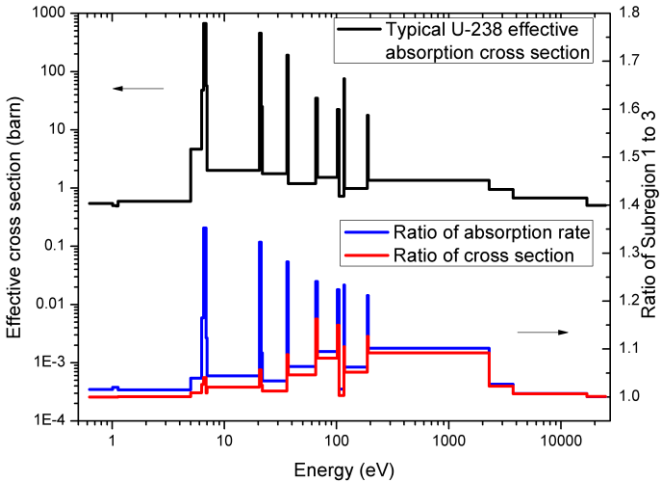

Fig. 4 Comparison of U-238 absorption cross section and rates between Subregions 1 and 3

Traditionally, resonance calculations have been performed in a 2-D geometry by neglecting the axial heterogeneity in generating the MG cross section. Although a 3-D transport capability (e.g., 3-D MOC) makes it possible to perform the resonance calculation for a consistent 3-D geometry, this significant extension of the direct transport method should be based on its necessity, given the computational burden for the 3-D transport kernel. Ref. [18] discusses the effect of the cross sections produced either by a 2-D MCNP calculation with axially reflective boundaries, or by a 3-D MCNP calculation of the realistic configuration. These cross sections are then fed to a deterministic solver for eigenvalue calculation. Table I shows the eigenvalue comparison by using the 2-D and 3-D cross sections for three typical LWR cases with significant axial heterogeneities. From the trivial eigenvalue difference between 2-D and 3-D cross sections, it can be concluded that a 2-D resonance calculation should be sufficient for a direct transport calculation of the LWR applications.

Table I Comparison of Eigenvalues

Case	3D-XS	2D-XS
1	1.29166	1.29170
2	1.36064	1.36066
3	1.29027	1.29028

1. PWR pin cell (full details) with axial boundary leakage
2. Hot BWR pin cell (distributed moderator densities)
3. Partially inserted control rod in 3x3 pin configuration

2. Resonance Interference

Resonance interference is a long-standing problem that arises from the overlapping in energy of cross sections from several resonance isotopes. Fig. 5 shows the cross section interference between U-235 and U-238 at 5eV-90eV. Since the RI table is often prepared for each resonance isotope independently, resonance interference is neglected at this step and treated at the MG level, e.g., using Bondarenko iteration as described in the WIMS code [19].

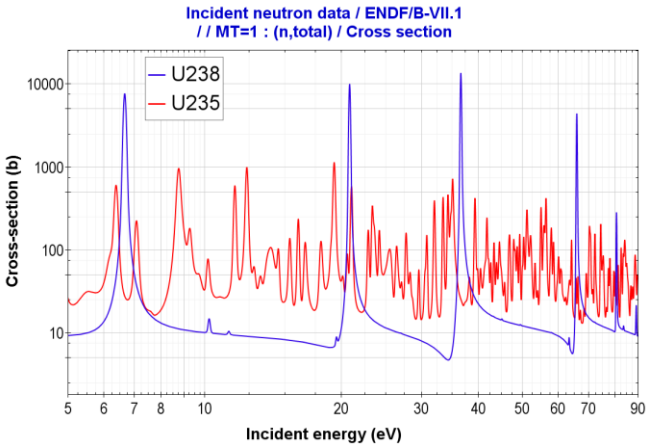

Fig. 5 Resonance interference between U-235 and U-238 [20]

However, it was shown in early research that corrections for the interference effect in the MG framework cannot resolve various conditions of the resonance overlap for a mixture of resonance isotopes [21]. It is necessary to utilize the CE cross section data to either predetermine the resonance interference factors (RIF) among resonance isotopes, or compute them on the fly [21]. Efforts were made to incorporate the interference effect by extending the dimension of the RI table or adding subgroup parameters using the density ratio of two resonance isotopes [22,23]. The difficulty for these methods occurs when the number of resonance isotopes becomes large, e.g., for MOX fuel or depleted fuel because the increased size of the RI table depends on the number and significance of the resonance isotopes in a specific problem. Alternatively, a heterogeneous pseudo-resonant isotope approach was proposed [24] to generate the RI table of a mixture that inherently includes the interference effect. However, similar practical issues are encountered when the number of isotopes is large and the fractions of them are various in the depletion calculation. To correct the interference effect on the fly, Ref. [25,26] discuss several successful methods based on the RIF model. The numerical results are included in Section III.

3. Miscellaneous Effects

Associated with the spatial self-shielding effect is the temperature distribution within a pin cell when thermal feedback is considered. In the conventional lattice calculation, an ‘effective temperature’ is chosen to replace the realistic temperature distribution of a fuel rod. Various approaches to obtain the effective temperature are discussed in Ref. [27]. However, the effective temperature model cannot be used if one wants to obtain accurate self-shielded

cross sections in every subregion of the fuel. Also, equivalence theory and ESSM cannot treat a non-uniform temperature distribution because of their inability to model within-pin effects. The subgroup method lacks a firm theoretical foundation to treat non-uniform temperature, so correction methods have been developed to account for the temperature distribution [28,29]. The numerical results for subgroup temperature correction is included in Section III.

Previously the focus of resonance calculation is on the resonance isotopes in the fuel pellet and burnable absorbers. A recent study showed that lack of self-shielding calculation for clad materials could introduce an eigenvalue error of 100-300 pcm [30]. Ref. [30] developed a simplified model by treating the clad region as an infinite slab, which efficiently yields accurate effective cross sections for clad isotopes using equivalence theory. For the subgroup method and ESSM/ESSM-X, since the background cross section of every resonant region can be determined by solving the MG fixed source problem (FSP), the self-shielding calculation of clad regions does not require extra efforts. However, to avoid the interaction between fuel and clad materials, separate resonance categories [6] should be used for the two materials, increasing the computational cost of solving the FSPs. In fact, all the resolved resonances of Zr isotopes are well within 100eV-0.1MeV (see Fig. 6), and only a few groups are present in this energy range for the typical group structure of ~50 groups normally used in direct transport methods. As a result, self-shielding calculation for the full resonance range (usually down to ~1eV) is not necessary for the category of Zr. Also, the resonance isotopes in the clad category are less-important than those of other categories, so a 1-group subgroup method was developed to perform a single group FSP for the less-important category such as clad [31]. The accuracy and efficiency of the 1-group subgroup is also discussed in Section III.

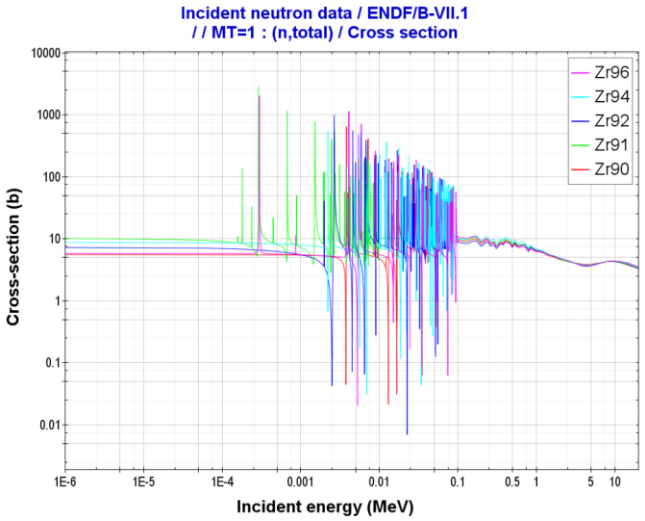

Fig. 6 Resonances of Zirconium isotopes [20]

4. Description of ESSM-X

ESSM-X [9] was originally developed to improve the accuracy of ESSM in treating temperature-dependent fuel subregions and resonance interference. The method performs a conventional ESSM calculation without subdivision of the fuel region to capture the inter-pin shielding effect. The resultant self-shielded cross sections are modified by correction factors incorporating the within-pin effects and resonance interference. These correction factors are computed through an efficient local quasi-1D slowing-down model, in which the inter-pin effect has been included by an equivalence cross section rather than an explicit boundary condition,

$$\left[\Sigma_{t,i}(u)+\Sigma_{eq,i}(u)\right]\phi_i(u)=\bar{Q}_i(u)+\Sigma_{eq,i}(u)\,. \qquad (2)$$

Eq. (2) is actually in a 0-D form, but 1-D information is embedded in $\Sigma_{eq,i}(u)$ and $\bar{Q}_i(u)$, the equivalent source and equivalence cross section of region *i*. Specifically, $\Sigma_{eq,i}(u)$ is derived from the CE fuel escape probability of region *i*,

$$P_{esc,i}(u)=\frac{\Sigma_{eq,i}(u)}{\Sigma_{t,i}(u)+\Sigma_{eq,i}(u)}\,. \qquad (3)$$

$\bar{Q}_i(u)$ is derived as the superposition of scattering sources of all fuel regions that contribute to region *i*,

$$\bar{Q}_i(u)=\frac{\Sigma_{t,i}(u)}{1-P_{esc,i}(u)}\sum_{j\in F}\frac{P_{i\to j}(u)}{\Sigma_{t,j}(u)}Q_j(u)\,. \qquad (4)$$

In Eq. (4), $P_{i\to j}$ is the first flight collision probability from region *i* to *j*, and $Q_j(u)$ is the regular scattering source that can be evaluated by numerically integrating the scattering kernel. Fig. 7 summarizes the calculation flow of ESSM-X.

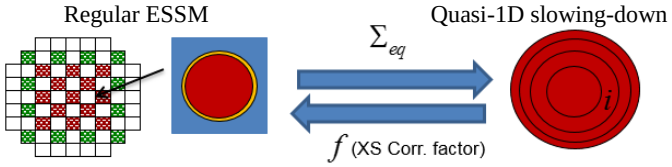

Fig. 7 ESSM-X calculation

III. RESULTS

We compare the subgroup method, ESSM and ESSM-X with regard to the important physics discussed in the previous section. The three methods are implemented in MPACT and the 56-group cross section library is used [17].

1. Spatial Self-shielding Effects

The spatially dependent absorption rates are compared for the three methods. For the case shown in Fig. 1, the radial variation of U-238 absorption rates of Pin 3 in the resonance energy range (0.6eV-25keV) are compared with MCNP. As previously addressed, ESSM is unable to resolve the within-pin effect, although one can solve a FSP with multiple fuel rings so that each ring obtains an individual equivalence cross section. Fig. 8 shows that ESSM underestimates by 15% the U-238 absorption rate at the fuel rim. This bias could lead to 30% underprediction of Pu-239 in the rim zone at 31 GWd/tU (Fig. 9) and a significant bias of power distribution along the fuel radius (Fig. 10). The errors with the subgroup method are much smaller, and ESSM-X shows the best match with MCNP results. For all three methods, the total absorption rates of U-238 integrated over the fuel rings are acceptable according to the table included in Fig. 8.

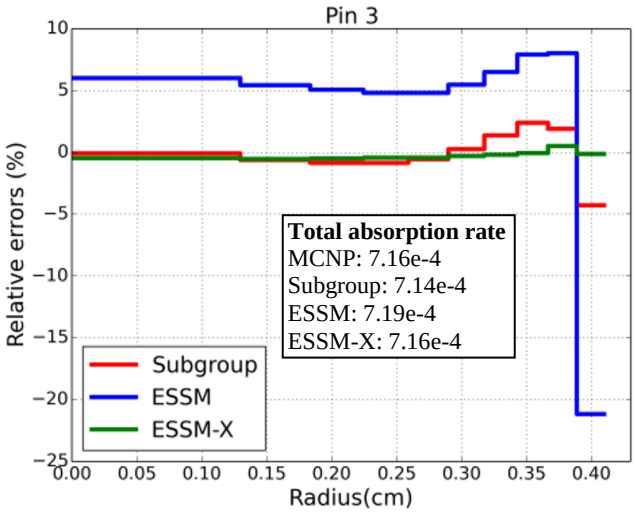

Fig. 8 Comparison of U-238 absorption rates in Pin 3

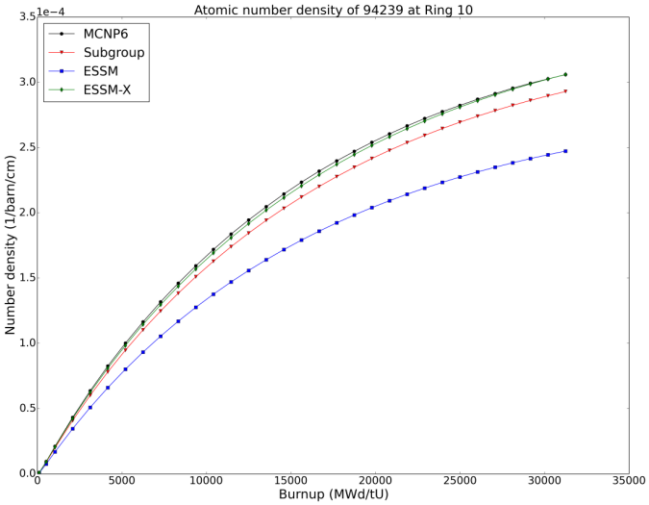

Fig. 9 Comparison of Pu-239 content in the rim zone

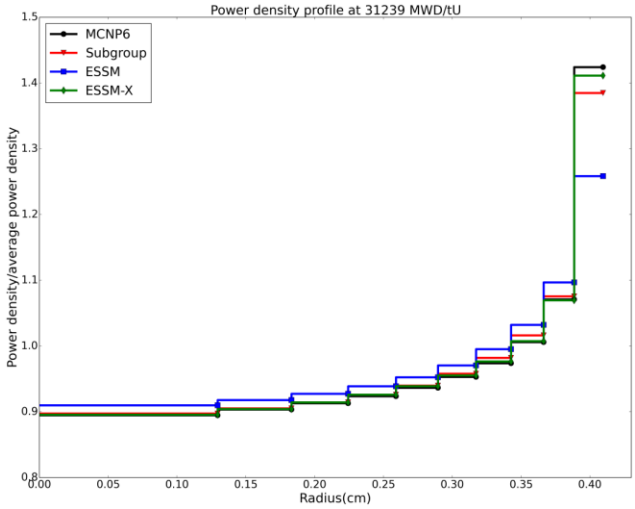

Fig. 10 Comparison of power distribution at 31.2 GWD/tU

In Section II.1, the azimuthal self-shielding is investigated. All three methods can be adapted to account for the azimuthal self-shielding by solving the FSP with the azimuthally refined mesh of Fig. 3. In Fig. 11, we compare the ratios of U-238 absorptions in subregions 1 and 3, predicted by MCNP and the three self-shielding methods. For the large resonances of U-238, all three methods predict the ratios accurately. ESSM and ESSM-X slightly underestimate the ratios for a few high energy resonances, but these resonances are less important. In general, all three methods are able to capture this effect acceptably.

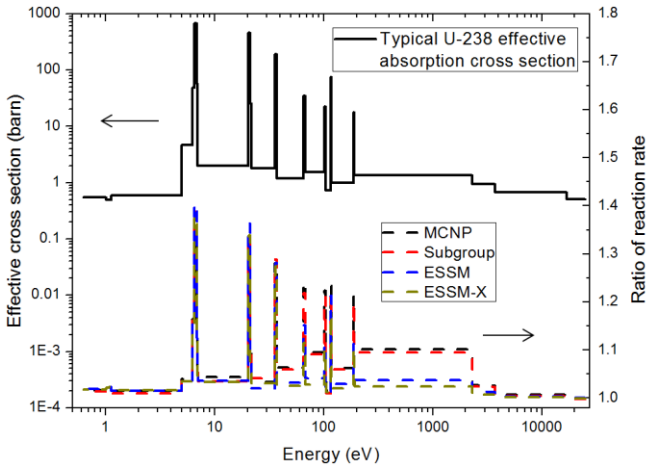

Fig. 11 Comparison of azimuthally dependent U-238 absorption rates

2. Resonance Interference

The resonance interference effect is investigated by comparing energy dependent reaction rates for key nuclides using the three resonance methods. Figs. 12 and 13 show the results of U-235 and Pu-239 for a MOX pin cell with 16 wt% Plutonium. Both ESSM and the subgroup method

model the resonance interference by Bondarenko iteration, which is unable to produce the correct reaction rates for U-235 and Pu-239 when multiple resonances are present. ESSM-X significantly improves the energy dependent reaction rates by using a correction factor based on solving the CE slowing-down equation.

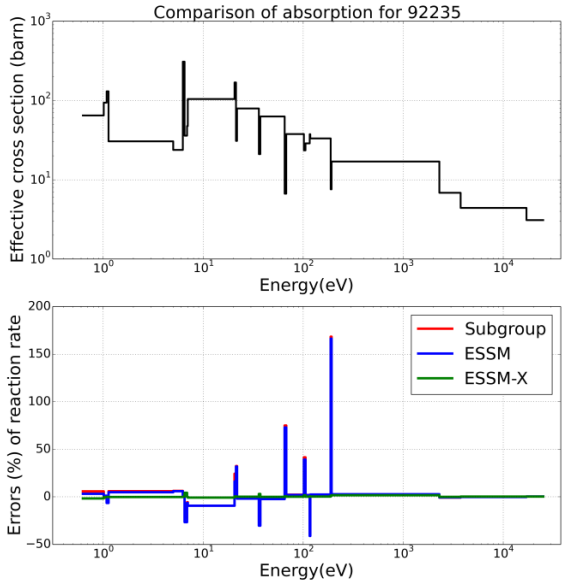

Fig. 12 Comparison of U-235 absorption rates for a MOX pin cell

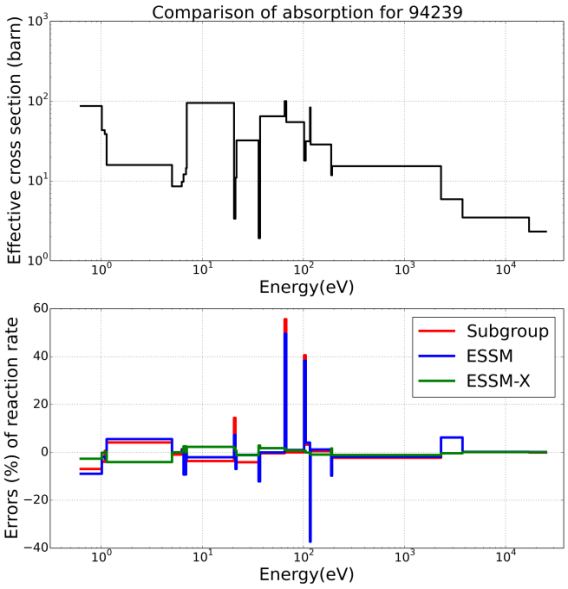

Fig. 13 Comparison of Pu-239 absorption rates for a MOX pin cell

3. Miscellaneous Effects

To study the non-uniform temperature effect, the subgroup method and ESSM-X analyze SNU's pin cell benchmark problems (the average temperature of each problem is shown in Fig. 13) [32]. In addition to the radially dependent reaction rates that have been presented previously, the fuel temperature coefficient (FTC) is also predicted. In Fig. 14 the significant discrepancy of the subgroup method as compared to MCNP is primarily due to the crude treatment of resonance interference, but in this analysis the slope of the curve (FTC) is more important. Because of linearly interpolating the CE cross sections among temperatures, the errors of the last two temperatures of ESSM-X become larger when the temperature grid is coarser at the high temperatures in the CE library. Other than that, both subgroup (with correction) and ESSM-X give reasonable estimates of FTC for the first five temperatures.

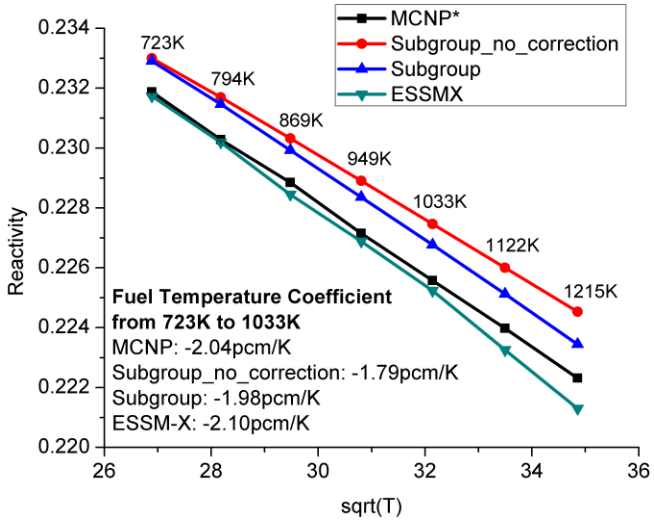

Fig. 14 Reactivity of non-uniform temperature pin cells
*The statistic error of MCNP results are all within 5 pcm (too small to view in the figure)

In Section II.3, the 1-group subgroup approximation is introduced to deal with the less important resonance categories such as clad. Table II shows the eigenvalue differences for VERA Progression Problems 1 and 2 [33] when the 1G subgroup is applied to different categories. From the '1G' column, we see an eigenvalue bias of -40 to -90 pcm when 1G subgroup is applied to all of the four predefined categories (two for uranium, one for clad and the other for absorbers). From the '1G-Clad' column, enabling 1G subgroup only for clad calculation is sufficiently good as compared to the standard MG subgroup. For some cases with resonance absorbers in a separate category (AgInCd in 2g, Gadolinium in 2o and 2p), we have small eigenvalue difference of ~20 pcm if using 1G subgroup for the two non-uranium categories ('1G-ButU' column). Given a total of four categories being used in our calculation, applying 1G approximation to any of the categories (such as clad) roughly saves 25% of the subgroup calculation time.

Table II Results of 1G subgroup compared to MG subgroup

Case	MG(k_{eff})	Eigenvalue difference (pcm) compared with MG		
		1G	1G-Clad	1G-ButU
1a	1.186242	-71.6	0.1	0.1
1b	1.181856	-79.5	0.1	0.1
1c	1.171485	-85.5	0.1	0.1
1d	1.162268	-79.1	0.1	0.1
2a	1.180841	-60.3	0.1	0.0
2b	1.182547	-67.9	0.1	0.1
2c	1.173164	-73.4	0.1	0.1
2d	1.164766	-67.3	0.1	0.1
2e	1.069116	-55.0	0.1	0.1
2f	0.975980	-51.1	0.1	0.1
2g	0.849946	-22.0	0.1	**22.7**
2h	0.791799	-37.2	0.1	0.0
2i	1.178756	-59.8	0.1	0.0
2j	0.975239	-51.1	0.1	0.1
2k	1.020060	-53.1	0.1	0.1
2l	1.017051	-49.8	0.1	0.0
2m	0.936860	-44.7	0.1	0.0
2n	0.868073	-42.7	0.1	0.0
2o	1.047530	-61.6	0.1	**-9.6**
2p	0.927848	-62.0	0.1	**-17.0**
2q	1.171205	-85.0	0.0	-0.1

4. Computing resources

A cross section library of ~50 groups is generally well within 50MB for storage of the cross section data, so the methods entirely based on multigroup cross section data such as equivalence theory, subgroup and ESSM, are generally satisfactory from a memory standpoint. Of the three methods, equivalence theory requires minimum computing time, since the calculations are analytic except for the evaluation of the Dancoff factor, which may require a single group transport sweep [34]. In contrast, subgroup and ESSM need to perform FSP calculations in each 2-D plane for every resonance group and category. Generally, the computing time of subgroup and ESSM is comparable, since ESSM needs ~4 iterations to converge the equivalence cross section, while subgroup solves for ~4 subgroup levels. Because of its use of CE cross sections to solve the slowing-down equation, ESSM-X is more expensive than the other methods.

Table III compares the computing time and memory demand of the three methods. Cases 1-4 represent the combinations of fresh/depleted fuel and coarse/fine mesh. The fine mesh FSP calculation utilized 10 radial rings in the fuel, a 0.01 cm ray spacing, 24 azimuthal angles per octant, and 4 polar angles. For the coarse mesh, the fuel is subdivided into 3 rings, and a 0.05/16/3 discretization is used for the MOC solver. In spite of the number of isotopes, four resonance categories are used for FSP calculations, so the computing times of subgroup and ESSM do not increase when the fuel is depleted. The additional time of ESSM-X compared to ESSM is modest (especially for the fine mesh), primarily due to solving the quasi-1D slowing-down equation. The memory demand and the efficiency of ESSM-X is sensitive to the number of isotopes, which determines the size of CE data loaded into the problem and the speed of slowing-down calculation. A merit of ESSM-X is that the pin-cell based slowing-down calculations are naturally decoupled, so the additional memory requirement for ESSM-X (~260MB for a depleted case) should be independent of the geometrical size of the problem. This also makes the model easy to be implemented in parallel.

Table III Computing resources of the resonance methods

	Reso. calc. time (s)			Memory (MB)		
	Sub.	ESSM	ESSM-X	Sub.	ESSM	ESSM-X
1	19.1	19.2	18.8	31.4	31.3	57.9
2	18.9	18.3	22.7	31.6	31.6	294
3	1.50	1.40	1.63	9.43	9.43	35.8
4	1.49	1.38	3.92	9.49	9.48	272

Case 1: fresh pin + fine mesh
Case 2: depleted pin (153 isotopes) + fine mesh
Case 3: fresh pin + coarse mesh
Case 4: depleted pin + coarse mesh

IV. CONCLUSION

This paper reviews the important physics that the resonance self-shielding method needs to account for in direct transport calculations. Table IV summarizes the features of the four resonance methods regarding their capability to resolve the physics of interest. As the fastest model, equivalence theory is not able to account for many of the important phenomena. The efficiency of the subgroup method and ESSM is comparable, but subgroup is superior in terms of modeling the physics correctly.

Table IV Comparison of resonance methods

Physics	Equivalence Theory	Subgroup	ESSM	ESSM-X
Inter-pin	√	√	√	√
Radial	×	O	×	√
Azimuthal	×	√	O	O
Interference*	×	×	×	√
Temperature	×	O	×	√

√ good O acceptable × problematic
*RIF model could make the first three methods better

As shown in the table, ESSM-X is a high-fidelity model. Recently, a similar approach that models the global and local self-shielding effects separately has also been successful by integrating equivalence theory with local slowing-down calculation [35]. In fact, any of the three multigroup-based methods (equivalence theory, the subgroup method and ESSM) can be combined with slowing-down calculation to improve the local accuracy.

Future work for these fusion-type methods is to improve the efficiency of the associated slowing-down calculation and to implement a better temperature model for CE cross sections.

In addition, it can be concluded from this paper that (1) the simplified clad self-shielding treatments are sufficient; (2) it is not necessary to perform the 3-D self-shielding calculation in PWR applications.

ACKNOWLEDGEMENTS

This research was supported by the Consortium for Advanced Simulation of Light Water Reactors (http://www.casl.gov), an Energy Innovation Hub (http://www.energy.gov/hubs) for Modeling and Simulation of Nuclear Reactors under U.S. Department of Energy Contract No. DE-AC05-00OR22725.

REFERENCES

1. R. E. MACFARLANE and D. W. MUIR, "NJOY99.0 Code System for Producing Pointwise and Multigroup Neutron and Photon Cross Sections from ENDF/B Data," Report PSR-80/NJOY99.0, Los Alamos National Laboratory, New Mexico (2000).
2. M. E. Dunn and N. M. Greene, "AMPX-2000: A Cross-Section Processing System for Generating Nuclear Data for Criticality Safety Applications," *Trans. Am. Nucl. Soc.*, 86, 118 (2002).
3. D. G. CACUCI (Ed.), *Handbook of Nuclear Engineering*, Lattice Physics Computations, Chapter 9, Springer, New York (2010).
4. K. SMITH and B. FORGET, "Challenges in the Development of High-Fidelity LWR Core Neutronics Tools," *Proc. M&C-2013*, Sun Valley, Idaho, May 5-9 (2013).
5. R. J. J. STAMM'LER and M. J. ABBATE, *Methods of Steady-state Reactor Physics in Nuclear Design*, Academic Press, London (1983).
6. R. J. J. STAMM'LER, et al., *HELIOS Methods*, Studsvik Scandpower (2003).
7. S. G. HONG and K. S. KIM, "Iterative Resonance Self-Shielding Methods Using Resonance Integral Table in Heterogeneous Transport Lattice Calculations," *Ann. Nucl. Eng*., 38, 32 (2011).
8. M. L. WILLIAMS and K. S. KIM, "The Embedded Self-shielding Method," *PHYSOR-2012*, Knoxville, TN, April 15-20, (2012).
9. Y. LIU, et al., "A Full Core Resonance Self-shielding Method Using a Continuous Energy Quasi-1D Slowing-down Solution that Accounts for Temperature-dependent Fuel Subregions and Resonance Interference," *Nucl. Sci. Eng*., 180, 247 (2015).
10. MPACT Team, "MPACT: User's Manual Version 1.0.0", November 8, 2013.
11. A. M. WEINBERG and E. P. WIGNER, *The Physical Theory of Neutron Chain Reactors*, University of Chicago Press, Chicago (1958).
12. R. GOLDSTEIN and E. R. COHEN, "Theory of resonance absorption of neutrons," *Nucl. Sci. Eng.*, 13, 132 (1962).
13. X-5 Monte Carlo Team, "MCNP-A General Monte Carlo N-Particle Transport Code, Version 5", LA-UR-03-1987, Los Alamos National Laboratory (2000).
14. Y. LIU and W. R. MARTIN, "Assessment of homogeneous and heterogeneous resonance integral tables and their applications to the embedded self-shielding method", *Ann. Nucl. Eng*., 92, 186 (2016).
15. C. STOKER and Z. WEISS, "Spatially Dependent Resonance Cross Sections in a Fuel Rod," *Ann. Nucl. Energy*, 23, 765 (1996).
16. H. MATSUMOTO, M. OUISLOUMEN and T. TAKEDA, "Development of Spatially Dependent Resonance Shielding Method," *J. Nucl. Sci Technol.*, 42, 688 (2005).
17. K. S. KIM, et al., "Automatic Coarse Energy Group Structure Optimization by Minimizing Reaction Rate Differences for the SCALE and CASL Code Systems," in reparation for M&C 2017.
18. Y. LIU and W. R. MARTIN, "Is 3-D Resonance Self-shielding Calculation Necessary for the Direct Transport Method in LWR Analysis?" *Trans. Am. Nucl. Soc.*, 113, 1125 (2015).
19. J. R. ASKEW, et al., "A General Description of the Lattice Code WIMS," J. British Nucl. Energy Soc., 5, 564 (1966).
20. N. SOPPERA, M. BOSSANT, E. DUPONT, "JANIS 4: An Improved Version of the NEA Java-based Nuclear Data Information System", *Nuclear Data Sheets*, 120, 294 (2014).
21. M. L. WILLIAMS, "Correction of Multigroup Cross Sections for Resolved Resonance Interference in Mixed Absorbers," *Nucl. Sci. Eng*., 83, 37 (1983).
22. K. S. KIM and S. G. HONG, "A New Procedure to Generate Resonance Integral Table with an Explicit Resonance Interference for Transport Lattice Codes", *Ann. Nucl. Energy.*, 38, 118 (2011).
23. Z. GAO, Y. XU and T. J. DOWNAR, "The Treatment of Resonance Interference Effects in the Subgroup Method," *Ann. Nucl. Energy.*, 38, 995 (2011).
24. T. ZU, et al., "Heterogeneous Pseudo-Resonant Isotope Method for Resolved Resonance Interference Treatment in Resonance Self-shielding Calculation," *Nucl. Sci. Eng*., 184, 495 (2016).
25. D. KNOTT and E. WEHLAGE, "Description of the LANCER02 Lattice Physics Code for Single-Assembly and Multibundle Analysis," *Nucl. Sci. Eng*., 155, 331 (2007).
26. Y. LIU, et al., "Modeling Resonance Interference by 0-D Slowing-down Solution with Embedded Self-shielding Method," *Proc. M&C-2013*, Sun Valley, Idaho, May 5-9 (2013).

27. W. J. M. de KRUIJF and A. J. JANSSEN, "The Effective Temperature to be Used for Calculating Resonance Absorption in a ^{238}UO2 Lump with Nonuniform Temperature Profile," *Nucl. Sci. Eng.*, 123, 121 (1996).
28. H. G. JOO, et al., "Implementation of Subgroup Method in Direct Whole Core Transport Calculation Involving Nonuniform Temperature Distribution," Proc. M&C-2005, Palais des Papes, Avignon, France, September 12-15 (2005).
29. C. A. WEMPLE, et al., "Improved Temperature-Dependent Resonance Treatment in HELIOS-1.9," *Trans. Am. Nucl. Soc.*, 96, 657 (2007).
30. S. CHOI, et al., "Resonance Self-shielding methodology of new neutron transport code STREAM," *J. Nucl. Sci. Technol.*, 52, 1133 (2015).
31. Y. LIU et al., "Runtime Improvements to the Cross Section Calculation in MPACT," CASL-I-2016-1105-000, CASL, May 31 (2016).
32. Y. JUNG and H. JOO, "Investigation of Intra-Pellet Temperature Profile Treatment in nTRACER Resonance Calculation," The 4th I-NERI meeting, South Korea, November 19 (2015).
33. A. GODFREY, "VERA Core Physics Benchmark Progression Problem Specifications," CASL-U-2012-0131-003, CASL (2014).
34. N. SUGIMURA and A. YAMAMOTO, "Evaluation of Dancoff Factors in Complicated Geometry using the Method of Characteristics," *J. Nucl. Sci. Technol.*, 43, 1182 (2006).
35. S. CHOI, D. LEE and C. LEE, "Improved Resonance Self-shielding Method Considering Resonance Scattering Effect," *PHYSOR-2016*, Sun Valley, ID, May 1-5, (2016).